JOURNAL OF SPACECRAFT AND ROCKETS
Vol. 41, No. 5, September–October 2004

Compact Energetic Light Particle Detector and Spectrometer

B. David Green* and Gary E. Galica†
Physical Sciences, Inc., Andover, Massachusetts 01810-1077
Takashi Nakamura‡
Physical Sciences, Inc., San Ramon, California 94583-1295
James D. Sullivan§
Boston University, Boston, Massachusetts 02215
Toshio Abe¶
Mitsubishi Electric Company, Kanagawa 247, Japan
Shinji Badono** and Shinji Murata**
Mitsubishi Electric Company, Hyogo 661-8661, Japan
and
Hirahisu Matsumoto,†† Hideki Koshiishi,†† Tateo Goka,†† and Yugo Kimoto††
National Space Development Agency, Ibaraki 305, Japan

We have developed a megaelectron-volt class energetic charged-particle spectrometer based on a novel configuration and processing algorithm. The National Space Development Agency of Japan has undertaken a program to develop a particle monitor capable of discriminating and measuring protons in the range from 0.9 to 150 MeV, electrons in the range from 0.5 to >10 MeV and alpha particles >8 MeV, all within a single sensor called the standard dose monitor. The goal is to utilize sensors with nearly identical design and performance on several simultaneous missions to develop a clearer understanding of particle energies and their variability as a function of solar activity, latitude, and altitude. To date, four flight model sensors have been delivered. The sensors are designed to detect accurately the higher-energy particles and high count rates present during active solar periods. In addition, this sensor exhibits extremely efficient discrimination between low-energy electrons and protons. The sensors have been calibrated over nearly their entire particle-energy range. The design is described and calibration data are compared with the results of a Monte Carlo sensor performance model.

Introduction

THE need to characterize the radiation environment of the Earth's magnetosphere is gaining ever-increasing importance. The orbital radiation environment causes multiple effects on spacecraft, including long-term degradation of advanced electronic components and solar arrays, single-event upsets/latchups in electronic circuitry, spacecraft charging, and human exposure during long-duration missions. The missions of many satellites now require operation in orbits with harsh radiation environments. In addition, electronics are becoming more susceptible to radiation effects as the trends toward smaller feature sizes and the use of commercial components continue.

The potential impact on mission performance can only be assessed from knowledge of the environment the spacecraft will encounter. The density and energy of the particles accelerated by the interaction of the solar wind particles with the Earth's magnetosphere vary temporally and spatially. Coordinated measurements from several satellites possessing particle spectrometers of comparable capabilities are required to assemble a more complete and global view of the magnetosphere and its interaction with the solar wind. In addition, whereas the most energetic particles are comparatively rare, they possess the greatest potential for damage, and they are the least well characterized by the current orbital monitors.

The National Space Development Agency of Japan (NASDA) has undertaken a program to develop a particle monitor capable of discriminating and measuring protons in the range from 0.9 to 150 MeV, electrons in the range from 0.5 to >10 MeV, and alpha particles >8 MeV, all within a single sensor called the standard dose monitor (SDOM). The goal is to utilize sensors with nearly identical design and performance on several simultaneous missions to develop a clearer understanding of particle energies and their variability as a function of solar activity, latitude, and altitude. The sensors are designed to detect accurately the higher-energy particles and high-count rates present during active solar periods. To date, we have delivered four flight model SDOMs: two for the NASDA Data Relay and Tracking Satellites (DRTS-W and DRTS-E), one for the NASDA Mission Demonstration Satellite 1 (MDS-1), and the fourth SDOM for the Japanese Experiment Module (JEM) of the International Space Station (ISS). The MDS-1 satellite, Tsubasa, was launched into a geosynchronous transfer orbit in February 2002. The DRTS satellite, Kodama, was launched into geostationary orbit in September 2002. The SDOM sensors on both satellites operated successfully on orbit and returned data.

The natural radiation environment is driven by the interaction of the Earth's magnetic field with energetic particles ejected from the sun and particles of galactic origin, creating the asymmetrically spatially structured magnetosphere. The trapped radiation belts consist of inner (dominated by protons with energies extending up to above 100 MeV and outer (dominated by electrons with energies extending up to a few megaelectron volts) belts. The upper energy limit of the electrons is not well determined, and its measurement and variability are two of the objectives of current programs. Measurements on the Combined Release and Radiation Effects Satellites (CRRES) observed instantaneous bursts of

Received 26 June 2001; revision received 3 March 2003; accepted for publication 26 August 2003.

*Executive Vice President, Research Division, 20 New England Business Center. Senior Member AIAA.
†Group Leader, Radiation Technologies, 20 New England Business Center.
‡Manager, Global Projects, 2110 Omega Road/Suite D. Member AIAA.
§Center for Space Physics, 725 Commonwealth Avenue.
¶325 Kamimachiya, Kamakura.
**Amagasaki City.
††2-1-1 Sengen Tsukuba City.

electrons with energy peaking at 15 MeV and extending to 50 MeV (Ref. 1).

Particle sensors will encounter very different types of radiation environments depending on orbit altitude and inclination, location and orientation of the sensor on the spacecraft, and the local magnetic field. The particle sensors developed and demonstrated on previous satellite missions reflect a wide variety of design approaches and the variety of environments expected to be encountered.

One of the early orbital proton sensors (S30 on the Diaman Allemande satellite in 1970) utilized two solid-state detectors to discriminate protons into three energy bins (5–46 MeV) in a large geometric G-factor configuration that also provided pitch angle information.[2] The high-energy alpha proton spectrometer sensor measured protons (1.2–100 MeV), alphas (1.6–500 MeV), and electrons (0.88–1.6 MeV) from an 800-km polar satellite starting in 1971, using Si detectors in a sequential order to provide differential energy dE from a thin detector times E (five thicker Si detectors, each 1 mm thick) for discrimination and energy resolution.[3] A scintillator-based anticoincidence detector and collimator defined the collection G factor. The proton–electron telescope aboard the IMP7 satellite in 1972[4] and the charged particle analyzer on spacecraft 1976-059A (Ref. 5) refined the same concept into a more compact design and provided valuable insights into magnetospheric processes. A series of lightweight energetic particle detectors was developed by the Jet Propulsion Laboratory, California Institute of Technology, for the planetary probes.[6] These open structures relied on temporal coincidence on several detectors to define particles within a selected acceptance angle cone. Use of an anticoincidence detector and collimator is beneficial for magnetospheric applications to decrease omnidirectional flux to manageable counting rates, especially during storms. An exclusively scintillator-based burst detection dosimeter sensor for electron and proton detection was deployed on the global positioning system satellites after 1982 (Ref. 7). A continuous record of the electron flux in two energy bins and protons in six bins up to 50 MeV is provided by the geostationary operational environmental satellites series of satellites using three solid-state silicon detectors (SSD) and Cerenkov sensors.[8]

The CRRES had several energetic particle sensors that significantly extended our understanding of the magnetospheric environment. The Proton–Electron Telescope (PROTEL) sensor[9] and the spectrometer for electrons and protons[10] used collimation and an anticoincidence detector to define the particle flux onto a series of SSDs. PROTEL used a permanent magnet to deflect electrons, thereby preventing their detection. Detection energy range is limited by proton propagation distance through the detector. PROTEL represents the current high-energy limit of an all-SSD detection approach: Protons of up to 100 MeV were detected by a stack of six large, low-noise solid-state detectors with a combined thickness of over 14 mm. The high-energy electron fluxmeter (HEEF), also on CRRES, represented the first use of both solid-state detectors and a scintillator in combination to extend the energy range.[11] HEEF detected electrons up to 10 MeV. The combined SSD/bismuth germinate BGO scintillator detection approach was extended in the High Sensitivity Telescope sensor launched on the POLAR satellite in 1996 (Ref. 12). This large G-factor sensor utilized simultaneous detection by three SSDs and a plastic scintillator to detect and discriminate electrons ($<$10 MeV), protons ($<$90 MeV), and alphas ($<$187 MeV). Logic based on multiple threshold discrimination levels in the detectors is used to perform energy analysis. The resolution and sensitivity of this well-characterized sensor has provided fascinating insight into magnetospheric dynamics. The IMAGE mission is beginning to provide fascinating insight into the magnetospheric dynamics of energetic particles $<$500 keV (Ref. 13).

The dose monitor (DOM) sensor on ETS-VI, launched in 1994, utilized an all SSD detection, with a thin dE detector widely separated from a six-SSD stack E detector, permitting electron ($<$5.8 MeV), proton ($<$45 MeV), alpha, and heavy ion detection. Its extended collimator provided a well-defined (0.0029 cm$^2 \cdot$ sr) G factor.[14]

SDOM Sensor

In this paper, we present a description of, and performance data from, a new single sensor to discriminate energetic, megaelectron volt electrons, protons, and alpha particles over a wide energy range and to measure their energies with 20% accuracy: the SDOM. SDOM uses the energy deposited in a combination of solid-state detectors and a plastic scintillator to distinguish and measure the energy of each incident particle. The sensor is designed so that electrons, protons, alphas, and heavier particles each create a unique combination of signals in the detectors that permits their identity and their energy to be determined.

For each particle, the charge pulse from each detector is amplified, and the peak signal is digitized. The digital signals from all detectors are compared against a table of the signals expected for each particle and energy. The particle is then identified and assigned to a specific particle-energy bin. The table is developed through ground calibrations and modeling to maximize throughput, accuracy, and unambiguous assignment. Rapid sampling and processing permit particle detection at rates in excess of 10^5/s. Sample accumulation times and the number of energy bins can be adjusted to specific satellite orbits and geometries before launch. The SDOM has been specifically designed to count at rates encountered during solar storms without pulse pileup. The design embodies many of the desirable features of past particle monitors, extends operation to higher energies and faster rates, and uses a novel processing/algorithm approach to permit accurate particle identity/energy assignment.

Design Approach

Our compact SDOM makes use of three SSDs of increasing thicknesses backed by a thick, low-Z scintillator. The SSDs provide low-energy differential and total energy detection, and the scintillator permits high-energy detection and discrimination. The first detector is kept as thin as possible so that particles produce signals in two detectors at energies near the sensor threshold, thereby enabling discrimination at as low an energy as possible. The electron hole pair signal increases until a particle has enough energy to penetrate all of the way through a given detector. On breakthrough, a signal appears on the next detector along the trajectory. Detector thicknesses are selected to optimize range and accuracy of the detector combination.

Figure 1 shows the sensor configuration. Ion-implanted, fully depleted silicon detectors from Micron Semiconductor, Ltd., of 134-, 300-, and 1000-μm thickness are located in close proximity, just behind the defining aperture and window. A 56-mm-thick doped plastic scintillator placed behind the SSD stack provides approximately 80-MeV proton range, with energies resolved up to 160 MeV. For electrons, the scintillator provides energy resolution up to 10 MeV. Electrons with $>$10 MeV energy penetrate through the scintillator. Electrons well above 50 MeV are detectable (but not resolved). The signal from the scintillator is measured by a pair of miniature rugged photomultiplier tubes (PMTs) operated at approximately 500 V and coupled to the scintillator via an optical gasket. The PMTs are selected to have matched optical performance and temperature dependence and to observe the scintillator deposition volume from opposite sides. The scintillator (except at the PMT interfaces) is coated with a vapor-deposited aluminum plating to increase optical collection efficiency. Modeling of the performance with ray tracing indicated that photon collection efficiency was uniform to within 30% over the volume of the scintillator. A thin Kapton® (12.7-μm thickness) window with 0.3-μm thick gold and 0.2-μm aluminum coatings is used to prevent visible and UV light, as well as lower-energy particles, from entering the detectors.

Particle geometric collection efficiency is defined by a collimator and aperture. By using a common sensor head with different collimators, we can easily customize the G factor for different orbits and missions. The G factor can be made as large as 0.3 cm$^2 \cdot$ sr, although values between 0.1 and 0.03 are more typical. The collimator and front plate of the sensor are made of Densalloy, a machinable tungsten alloy with a density of 18.1 g/cm^3. For the detector sidewall structure, 5-mm-thick aluminum was used. To further decrease spurious detection of particles from outside the collimator acceptance

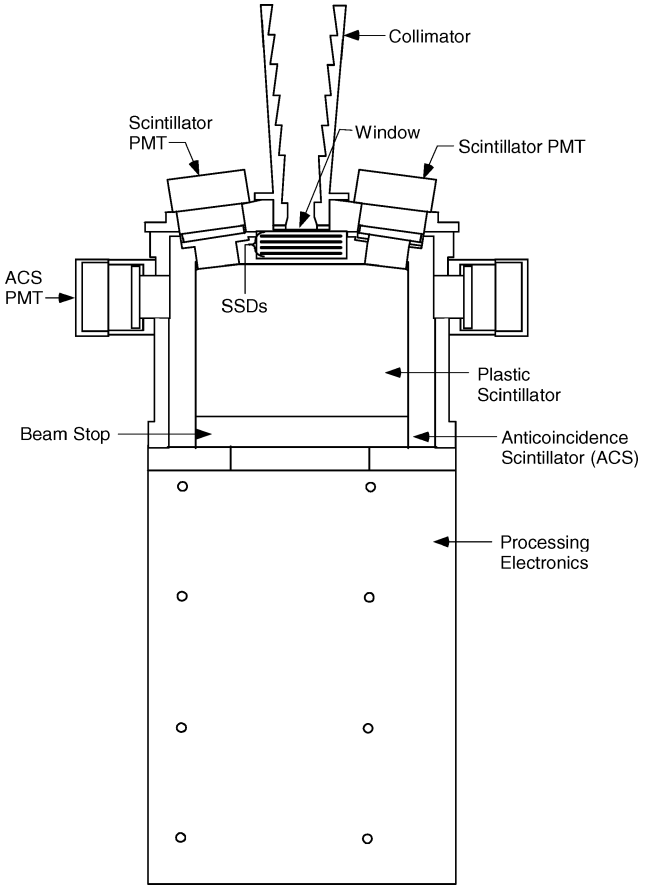

Fig. 1 Cross-sectional view of MDS-1 SDOM.

cone, the entire SSD package and front and side scintillator areas are surrounded by a 10-mm-thick aluminized plastic anticorrelation scintillator (ACS). Emission from the ACS is detected by another pair of matched miniature PMTs. The rear of the scintillator is well shielded by a dense beam stop, as well as by the SDOM electronics section and chassis. Preamplifier electronics are mounted directly above the detectors on the front plate of the sensor, with the amplifiers, digitizers, and logic circuits connected directly to the rear of the sensor. The entire assembly is mounted on a lightweight base, weighs less than 8 kg, and measures $121 \times 147 \times 322$ mm^3. The sensor head and electronics are about equal in weight and volume. Figure 2 shows a photograph of the sensor.

The sensor is designed to be in good radiative and thermal contact with the host spacecraft. External surfaces are painted black to maximize radiation, and a thermally conductive shock absorbing material cushions the entire base of the SDOM. The front external cover (facing space) has a silver/inconel optical solar reflector applied to minimize SSD/sensor operating temperature changes due to solar heating. Portions of the sensor were designed and fabricated both in the United States and in Japan in a true international team collaboration.

The processing electronics are data driven, with event detection being triggered by any detector, each having independently adjustable trigger threshold voltages. Each detector, including the ACS, has its own trigger threshold that can be commanded from the ground. If the signal in any SSD or scintillator detector exceeds that detector's threshold, and the ACS detector is below its threshold, that event is processed as a potential particle. The processor will subsequently determine whether that event constitutes a true particle or whether it is a spurious or rejected event.

Electronics were developed to sample the signals from all detector channels simultaneously at 100-ns resolution, determine peak signals in each channel, and compare the digitized (8-bit) signals to assign particle type and energy via algorithms discussed in the next section.

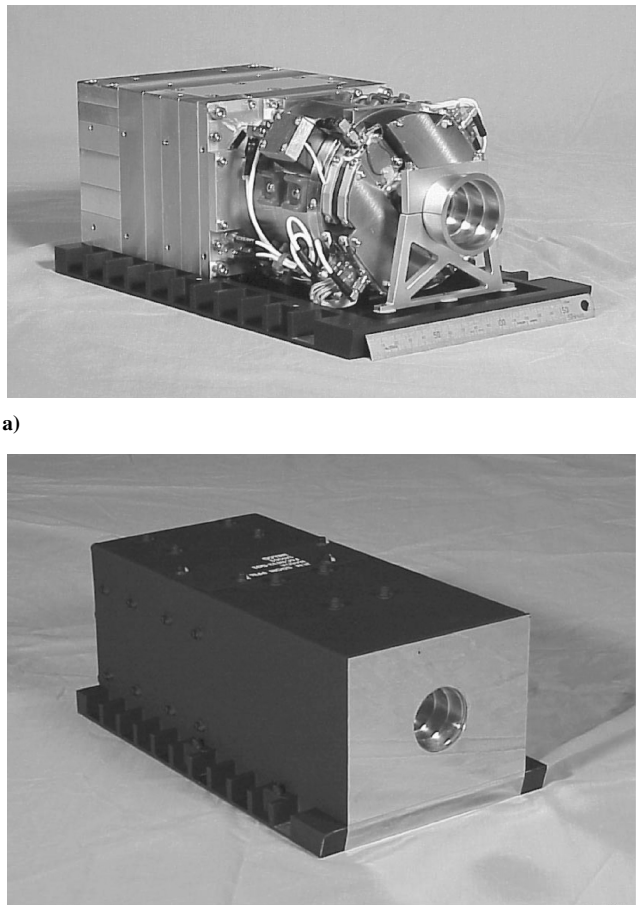

a)

b)

Fig. 2 Photograph of JEM SDOM: a) with cover removed and b) with cover installed.

The processing of signals with parallel field programmable gate arrays enables rapid particle detection, discrimination, and energy assignment at rates in excess of 200 kHz. These rates will permit accurate measurements of orbital particle fluxes during periods of elevated fluxes associated with severe solar activity. The total power consumed by the sensor during continuous operation is 13 W.

Hardware Development Program and Test Results

The sensor assembly and handling follows strict quality assurance guidelines. Fabrication is to level MIL-STD-975 using high reliability parts (grade 2 or better) and materials selected for radiation tolerance and low outgassing (<1% total mass loss, <0.1% collected volatile condensable materials). After sensor and electronics integration, preliminary bench testing to establish SDOM response and noise characteristics is completed. Radioisotope sources ($Sr^{90} 9 \times 10^{-8}$ Ci and $Rb^{106} 9 \times 10^{-7}$ Ci) produce energetic (beta) electrons with cutoff energies of 2.282 and 3.54 MeV, respectively. These sources are used to produce signals in all detectors and to check counting rates and analog signal levels.

The first engineering model was subjected to qualification-level environmental testing. Although most of the SDOM components have space heritage, to our knowledge, the Hamamatsu R5600 (and R7400) miniphotomultiplier tubes do not. These parts were qualified by testing separately to vibration levels of 20-g sine sweep and random and to 1000-g shock (1-ms half-sine). No damage or performance degradation at the 5% level was detected from vibration, shock, or thermal cycling. The tubes were also subjected to Co^{60} gamma irradiation to 10^4 Gy. We observed no detectable change in dark current and less than 10% decrease in responsivity after irradiation.

The entire SDOM sensor and electronics were subjected to vibration (sine and random at 20-g) and 1000-g shock with no damage or

degradation. Thermal cycle testing over a −55°C to +65°C survival range, with eight −45°C to +55°C operational cycles also showed no damage, with starts at −55°C and +65°C completely successful. At +55°C, the SSD detectors exhibited about 15% increased noise over room-temperature operation. Electromagnetic interface testing of radiated and conducted emissions and susceptibility demonstrated that the electronics had a good design with proper filtering. Subsequent sensors have been fabricated and tested to levels appropriate for their specific missions, including DRTS, MDS-1, and JEM of the ISS.

Sensor Operation and Algorithm

Based on measurements of the amplifier gains, we predict the signals from each detector using a sophisticated, physics-based Monte Carlo model that incorporates the known geometry and materials of the sensor, the measured electrical performance (preamplifier gain and noise) and the GEANT code developed at the European Organization for Nuclear Research.[15] Simulation of the trajectories and interactions for ensembles of electrons (0.1–50 MeV), protons (0.5–250 MeV), alphas, and representative heavy ions yield very accurate energy deposition distributions. For less demanding tasks, we also use a simple, non-Monte Carlo engineering code based on measured energy depositions for electrons,[16] protons, and alphas.[17]

Rather than use a threshold-based particle discrimination and energy assignment approach, we developed a pulse-height analysis approach that utilizes the absolute magnitude of the signals from all detectors. As particle energy increases, the signal in a detector increases until there is sufficient range that the particle breaks through and reaches the next detector. We have developed algorithms that use the signals from the penetrated detectors as the prime determinant of particle identity, and the signal from the unpenetrated detector as the prime determinant of energy. All detectors must be consistent with the identity-energy assignment. This effect is shown in Fig. 3, where the signals produced by protons in SDOM SSD and scintillator detectors are plotted as a function of energy. Most often, protons propagate through the SSD detector stack and scintillator with only a modest off-axis scattering component. Protons with energies above 90 MeV penetrate through the scintillator. Protons at higher energies are resolved, but with somewhat lower resolution. Electrons undergo significantly more scattering, broadening their energy deposition in each detector.

The modeled energy spread from an ensemble of monoenergetic particles is used to set expected signal magnitudes and widths, which in turn drive the particle counting bins' energy ranges. The magnitudes of the acceptable signals are adjusted to be consistent with scattering distributions and noise levels determined from the detailed modeling and from calibration. A wide range of penetrated SSD detector signals may satisfy the logic conditions as long as the value lies in the range consistent with that particle identification. The amplified, digitized signals from each detector are sequentially compared with tabulated values for each particle energy bin. The number of particle-energy bins can be as high as 64; however, more

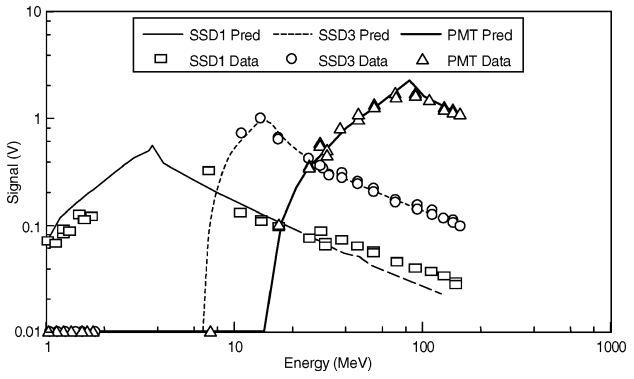

Fig. 3 Proton calibration data of signal in SSDs and scintillator acquired at three different facilities (also energy deposition predictions from GEANT code for SDOM based on our geometries and amplifier gains).

Table 1 Calibrations performed during SDOM development

Energy, MeV	Facility
	Proton
0.9–1.7	NASA Goddard Space Flight Center Radiation Effects Facility
7.5–31	Yale University Wright Nuclear Structure Laboratory
29–159	Harvard Cyclotron Laboratory
	Electron
0.4–1.8	NIST Van de Graaff
7–32	NIST Medical Industrial Research Facility
	Alpha
10–50	Yale University Wright Nuclear Structure Laboratory
	Carbon
15–120	Yale University Wright Nuclear Structure Laboratory

typical values are 32 or 25 depending on each spacecraft's mission requirements and available telemetry bandwidth. A typical 32-bin configuration provides 7 electron bins, 15 proton bins, 6 alpha bins, and 4 diagnostic bins. A 25-bin configuration includes 5 electron, 12 proton, 4 alpha, and 4 diagnostic bins.

We implement the processing algorithm using several field programmable gate arrays (FPGAs). As a particle enters the sensor and triggers an SSD or the scintillator, signals from each detector's shaping preamplifier are read and digitized every 80 ns. The maximum signal is determined and processed by the FPGAs to determine particle identity and energy. Processing is complete, and a new particle can be measured within 5 μs, as demonstrated by bench testing and during calibration. Each detector's signal must lie between (greater than or equal to the lower value, less than the higher value) the entries in the table for an assignment (and the ACS must have produced no significant signal). The detector signals are tested against the values for every bin to find whether a unique determination has occurred. If the detector signals are compatible with two or more bins, the particle is counted as uncertain, and that particle is recorded in one of the diagnostic bins. The purpose of ground calibrations and modeling is to set the values of the look-up table (LUT) used by the algorithms and to eliminate any nonunique determinations.

Over its development cycle (from benchtop prototype, to engineering model, to several flight models) we have calibrated SDOM over nearly its entire particle-energy range. Calibrations were performed for protons over the 0.9–160-MeV range, electrons over the 0.4–32-MeV range, alphas over the 10–120-MeV range, and carbon (representing heavy ions) over the 15–120-MeV range at several facilities. The calibration energies are summarized in Table 1.

The model includes the full three-dimensional geometry of the sensor and surrounding spacecraft. Using the model in conjunction with calibration data, we assess various background and interference effects, such as x-ray production in the sidewalls and collimator, shielding effectiveness, and ACS efficiency.

Sensor Performance

Because the SDOM sensor model is entirely physics based, comprising only known and independently measured quantities, and no free parameters, it is an extremely useful tool for interpreting calibration data and future flight data. The model incorporates the sensor geometry, materials properties, electronic noise, preamplifier gain, and algorithm logic. We have used the calibration data to validate this model. We compare the SDOM response to well-characterized particle input to the model predictions, including analog detector signals, as well as the results of the internal algorithm processing. Because the model is entirely physics based, we can use the validated model with confidence to interpolate and extrapolate the sensor performance to particle–energy regions that are uncalibrated.

One of the benefits of the SDOM algorithm is its excellent specificity. Its specificity derives from four independent criteria having to be met (three SSD signals and one scintillator signal) for an assignment to be made. If even one of the criteria is not met, then that particle is rejected. Specificity is important, especially for discriminating against low-energy electrons in the orbital environment.

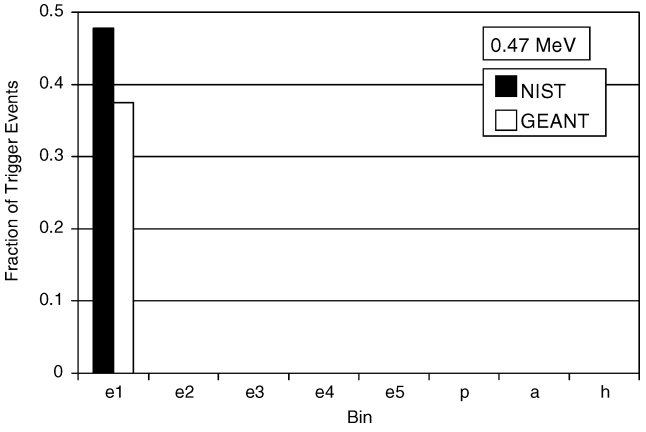

Fig. 4 Processed data resulting from irradiation with 0.47-MeV electrons.

In many orbits, electrons dominate the incident particle flux over protons, sometimes by orders of magnitude. To prevent misinterpretation of the proton flux, a flight sensor should not misassign low-energy electrons as protons. SDOM has demonstrated electron rejection of better than 1000:1. That is, less than 0.1% of incident electrons are misassigned as protons. Figure 4 shows an example of this excellent rejection. These data were acquired at the National Institute of Standards and Technology (NIST) Van de Graaff generator. Figure 4 shows the processed data resulting from irradiation with 0.47-MeV electrons compared to GEANT predictions. Figure 4 displays the resulting energy spectrum where bins $e1$–$e5$ correspond to electron energies of 0.3–>10 MeV, spaced logarithmically, the P bin is the sum of all protons bins (bins P1–P12), the A bin is the sum of all alpha bins (bins A1–A4), and H is the heavy bin. During this calibration, no electrons were misassigned as protons, alphas, or heavy ions, thereby yielding the upper limit 0.1% of electron contamination. This result agrees with the sensor model predictions.

We have also calibrated SDOM with high-energy electrons (7–32 MeV). Electrons with energies >10 MeV penetrate completely through the scintillator. For electrons between 10 and 32 MeV, the energy detected in the scintillator is constant. These calibration results are in good agreement with the GEANT model predictions.

After the sensor model is validated with calibration data, we use that model to predict the geometric factor and cross-contamination for each particle–energy bin. The reported G factors are weighted for an E^{-3} orbital flux distribution. The E^{-3} distribution is a reasonable approximation to the orbital spectrum.

To interpret the orbital data, the analyst uses the following procedure. The number of particles detected in each particle–energy bin during each sample time N_i is given by

$$N_i = t_{\text{sample}} \int_0^{\infty} F(E) G_i(E)\, \mathrm{d}E \tag{1}$$

where t_{sample} is the sample time, $F(E)$ is the omnidirectional orbital flux expressed in particles per square centimeter per steradian per megaelectron volt per second, and $G_i(E)$ is the geometric factor for the ith bin expressed in square centimeters steradian.

This integral is approximated by

$$N_i = t_{\text{sample}} F(E_{\text{av}}) G_i^W \text{FWHM}_i \tag{2}$$

where $F(E_{\text{av}})$ is the omnidirectional flux at the average bin energy (weighted by the E^{-3} orbital flux), G_i^W is the E^{-3} weighted average geometric factor, and the full-width half-maximum (FWHM) energy is given in terms of the ith bin. G_i^W, FWHM_i, and t_{sample} are the calibration constants for the sensor. Those calibration constants for the MDS-1 SDOM are summarized in Table 2.

The sensor performance is also shown graphically in Figs. 5 and 6. Figure 5 shows the energy resolution ($\mathrm{d}E/E$) for all of the proton, electron, and alpha bins for the MDS-1 SDOM. The MDS-1 energy resolution is limited by the number of bins available in the telemetry data (in this case, 25). Calibration data show that the inherent

Table 2 Calibration constants and performance parameters for the MDS-1 SDOM

Bin	Average energy, MeV	FWHM, MeV	E low, MeV	E high, MeV	G factor, $\text{cm}^2 \cdot \text{sr}$
			Proton		
P1	1.02	0.23	0.91	1.14	0.00312
P2	1.29	0.42	1.08	1.50	0.01147
P3	1.73	0.54	1.46	2.01	0.00891
P4	2.33	0.73	1.96	2.70	0.01076
P5	3.20	1.07	2.66	3.74	0.00903
P6	4.55	1.66	3.73	5.38	0.01104
P7	6.85	2.25	5.73	7.98	0.00985
P8	10.9	8.62	6.59	15.2	0.00689
P9	18.4	15.8	10.5	26.3	0.00685
P10	32.2	21.7	21.4	43.0	0.00627
P11	56.9	37.8	38.0	75.8	0.01196
P12	148	125	85.9	210	0.03152
			Electron		
E1	0.62	0.58	0.40	0.91	0.00102
E2	1.45	1.13	0.89	2.02	0.00274
E3	3.97	3.60	2.17	5.77	0.00271
E4	8.02	3.33	6.36	9.69	0.00486
E5			10.0	>20	0.00588
			Alpha		
A1	9.24	5.40	6.51	11.9	0.01259
A2	18.4	11.0	12.9	23.9	0.00940
A3	34.9	16.8	26.5	43.3	0.00797
A4	11	72.1	65.1	137	0.01395
			Heavy ion		
H			1.5/nucleon	>60/nucleon	0.011

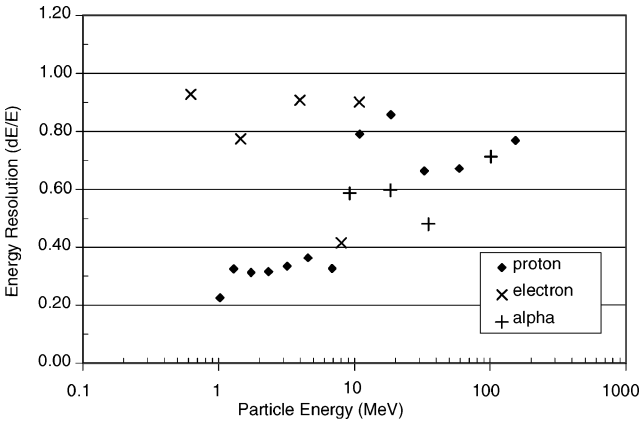

Fig. 5 Energy resolution (dE/E) for proton, electron, and alpha particle bins; MDS-1 SDOM; Table 1.

energy resolution for protons for this sensor is approximately 20%, which could support as many as 27 proton bins. We have purposely positioned the proton energy bins to have finer resolution at lower energy, where the majority of the proton flux lies, and coarser resolution at high energy, where there are fewer protons. The electron and alpha resolutions are also limited by the number of bins available. The inherent energy resolution for alphas is similar to that for protons. The inherent energy resolution for electrons is somewhat coarser than that of protons and is approximately 50%.

The G factors for all bins are shown graphically in Fig. 6. For comparison, the geometric, or unit efficiency, G factor is 0.011 $\text{cm}^2 \cdot \text{sr}$. For protons and alphas, SDOM has nearly unit efficiency. The efficiency is lower for the lowest energy protons and for protons in bins P8, P9, and P10 (7–43 MeV). The efficiency for high-energy protons (>85 MeV) is actually higher than geometric because particles at those energies penetrate through the collimator. The efficiency for electrons is somewhat less than that for protons and alphas, running between 10 and 50% of geometric. This lower efficiency is caused by the high specificity of the sensor. The electron bins are developed purposely to provide high specificity at the cost of some efficiency.

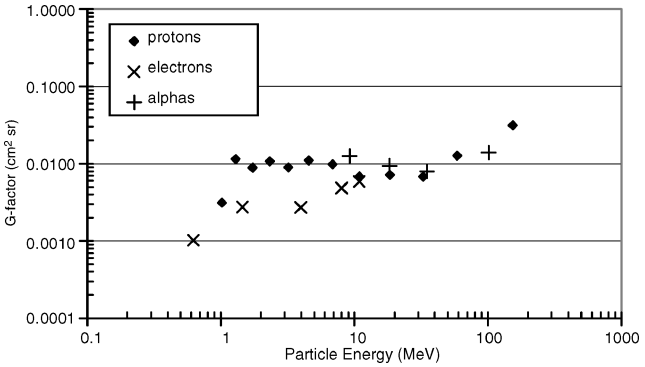

Fig. 6 *G* factors for proton, electron, and alpha particle bins; MDS-1 SDOM; Table 1.

Another salient feature of the SDOM architecture is its high level of redundancy available by virtue of the LUT algorithm architecture. As mentioned earlier, the scintillator has redundant photomultiplier tubes, each with its own preamplifier. The stack of three SSDs is integral to the design and cannot be fully redundant. However, SDOM supports up to 16 ground-commandable LUTs. By careful utilization of these LUTs, we have built a high level of redundancy into the system. SDOM includes LUTs optimized, so that the sensor will still operate with one or more detector failures. There are also several LUTs designed as diagnostic modes.

Although each PMT has roughly matched performance, there are enough differences between them that we have provided individually optimized LUTs for PMT0 and PMT1. As described earlier, SDOM is equipped with both electronic and optical internal calibrations. Under normal operating conditions, these calibration pulses produce a unique bin assignment when SDOM is commanded to use one of the diagnostic LUTs.

Conclusions

We have developed a series of compact sensors that permit high rate accurate energetic particle measurements on satellites. Both particle distributions and signals from individual particles will be available for analysis. The response of the sensors has been accurately characterized through extensive calibrations at several facilities and through performance during environmental testing. Once launched, this series of sensors should provide insight into the energetic distribution of energies and flux rates of ~0.5–200 MeV for particles at a variety of orbital stations.

Acknowledgment

The authors acknowledge the assistance of Joy Stafford-Evans during the design and testing of the standard dose monitor.

References

[1]Blake, J. B., Kolasinski, W. A., Fillius, R. W., and Mullen, E. G., "Injection of Electrons and Protons with Energies of Tens of MeV into L < 3 on 24 March 1991," *Geophysics Research Letters*, Vol. 19, No. 8, 1992, pp. 821–824.

[2]Fischer, H. M., Auschrat, V. W., and Wibberenz, G., "Angular Distribution and Energy Spectra of Protons of Energy 5 < E < 50 MeV at the Lower Edge of the Radiation Belt in Equatorial Latitudes," *Journal of Geophysical Research*, Vol. 82, No. 4, 1977, pp. 537–547.

[3]Reagan, J. B., Bakke, J. C., Kilner, J. R., Matthews, J. D., Imhof, W. L., "A High Resolution, Multiple Particle Spectrometer for the Measurement of Solar Particle Events," *IEEE Transactions on Nuclear Science*, Vol. 19, No. 1, 1972, pp. 554–561.

[4]Sarris, E. T., and Krimingis, S. M.,"Observations of Magnetospheric Bursts of High-Energy Protons and Electrons at 35 R_E with Imp 7," *Journal of Geophysical Research*, Vol. 81, No. 13, 1976, pp. 2341–2355.

[5]Baker, D. N., Belian, R. D., Higbie, P. R., and Hones, E. W., "High-Energy Magnetospheric Protons and Their Dependence on Geomagnetic and Interplanetary Conditions," *Journal of Geophysical Research*, Vol. 84, No. A12, 1979, pp. 7138–7154.

[6]Stone, E. C., Vogt, R. E., McDonald, F. B., Teegarden, B. J., Trainor, J. H., Jokipii, J. R., and Webber, W. R., "Cosmic Ray Investigation for the Voyager Missions; Energetic Particle Studies in the Outer Heliosphere and Beyond," *Space Science Reviews*, Vol. 21, 1977, pp. 355–376.

[7]Cayton, T. E., Higbie, P. R., Drake, D. M., Reedy, R. C., McDaniels, D. K., Belian, R. D., Walker, S. A., Cope, L. K., Noversfe, E., and Baca, C. L., "BDD-1: An Electron and Proton Dosimeter on the Global Positioning System," Final Rept., Los Alamos Rept. LA12275, UC-744, Los Alamos, NM, May 1992.

[8]Sellers, F. B., and Hanser, F. A., "A Design and Calibration of the GOES-8 Particle Sensors: EPS and HEPAD," *GOES-8 and Beyond*, Vol. 2812, Society of Photo-Optical Instrumentation Engineers, Bellingham, WA, 1996, pp. 353–364.

[9]Violet, M. D., Lynch, K., Redus, R., Riehl, K., Boughan, E., and Hein, H., "Proton Telescope (PROTEL) on the CRRES Spacecraft," *IEEE Transactions on Nuclear Science*, Vol. 40, No. 2, 1993, pp. 242–245.

[10]Nightingale, R. W., Vondrak, R. R., Gaines, E. E., Imhof, W. L., Robinson, R. M., Battel, S. J., Simpson, D. A., and Reagan, J. B., "CRRES Spectrometer for Electrons and Protons," *Journal of Spacecraft and Rockets*, Vol. 29, No. 4, 1991, pp. 614–617.

[11]Dichter, B. K., Hanser, F. A., Sellers, B., and Hunerwadel, J. L., "High Energy Electron Fluxmeter," *IEEE Transactions on Nuclear Science*, Vol. 40, No. 2., 1993, pp. 252–255.

[12]Blake, J. B., Fennel, J. F., Fiesen, L. M., Johnson, B. M., Kolasinski, W. A., Mabry, D. J., Osborn, J. V., Penzin, S. H., Schnauss, E. R., Spence, H. E., Belian, R., Fritz, T. A., Ford, W., Laubscher, B., Stiglich, R., Baraze, R. A., Hilsenrath, M. F., Imhof, W. L., Kilner, J. R., Mobilia, J., Voss, D. H., Korth, A., Gull, M., Fisher, K., Grande, M., and Hall, D., "CEPPAD, Comprehensive Energetic Particle and Pitch Angle Distribution Experiment on POLAR," *Space Science Reviews*, Vol. 71, 1995, pp. 531–562.

[13]Burch, J. L., Green, J. L., and Fuselier, S. A., "Mission Allows Magnetospheric Physicists to 'See' the Invisible," *EOS*, Vol. 82, No. 22, 2001, p. 241.

[14]Goka, T., Matsumoto, H., Fukuda, T., and Takagi, S., "Space Environment and Effects Measurements from the ETS-VI Satellite" (submitted for publication).

[15]Brun, R., Hagelburg, R., Hansroul, M., and Lasalle, J. C., "GEANT: Simulation Program for Particle Physics Experiments," European Organization for Nuclear Research, Rept. CERN-DD-78-2REV, July 1978.

[16]Berger, M. J., and Seltzer, S. M., "Stopping Powers and Ranges of Electrons and Positrons," National Bureau of Standards, Rept. NBS IR 82-2550 PB83-100289, Aug. 1982.

[17]Janni, J. F., "Proton Range-Energy Tables, 1keV–10GeV," *Atomic Data and Nuclear Data Tables*, Vol. 27, March–May 1982, pp. 147–339.

D. L. Cooke
Associate Editor